© 2017. Published by The Company of Biologists Ltd | Journal of Cell Science (2017) 130, 3399-3413 doi:10.1242/jcs.202127

RESEARCH ARTICLE

The *CCR2* 3′UTR functions as a competing endogenous RNA to inhibit breast cancer metastasis

Jinhang Hu[1,2], Xiaoman Li[3], Xinwei Guo[1,2], Qianqian Guo[1,2], Chenxi Xiang[1,2], Zhiting Zhang[1,2], Yingying Xing[1,2], Tao Xi[1,2,*] and Lufeng Zheng[1,2,*]

ABSTRACT

Diverse RNA transcripts acting as competing endogenous RNAs (ceRNAs) can co-regulate each other's expression by competing for shared microRNAs. CCR2 protein, the receptor for CCL2, is implicated in cancer progression. However, we found that a higher *CCR2* mRNA level is remarkably associated with prolonged survival of breast cancer patients. These conflicting results prompted us to study the non-coding function of *CCR2* mRNA. We found that the *CCR2* 3′ untranslated region (UTR) inhibited MDA-MB-231 and MCF-7 cell metastasis by repressing epithelial–mesenchymal transition (EMT) *in vitro*, and suppressed breast cancer metastasis *in vivo*. Mechanistically, the *CCR2* 3′UTR modulated the expression of the RhoGAP protein STARD13 via acting as a STARD13 ceRNA in a microRNA-dependent and protein coding-independent manner. The *CCR2* 3′UTR blocked the activation of RhoA–ROCK1 pathway, which is the downstream effector of STARD13, and thus decreased the phosphorylation level of myosin light chain 2 (MLC2) and formation of F-actin. Additionally, the function of the *CCR2* 3′UTR was dependent on STARD13 expression. In conclusion, our results confirmed that the *CCR2* 3′UTR acts as a metastasis suppressor by acting as a ceRNA for STARD13 and thus inhibiting RhoA–ROCK1–MLC–F-actin pathway in breast cancer cells.

This article has an associated First Person interview with the first author of the paper.

KEY WORDS: CCR2, 3′UTR, ceRNA, Metastasis, Breast cancer

INTRODUCTION

Worldwide, breast cancer is the most common malignancy among women (Sui et al., 2015). Metastasis is a complex process leading to dissemination of cancer cells from the primary tumor to distant organs (Gilkes et al., 2014), and it is the cause of the vast majority of deaths of patients with breast cancer (Papageorgis et al., 2015). Thus, there is an urgent need to elucidate the molecular mechanisms contributing to breast cancer metastasis.

CCL2 is a member of the CC chemokine family and acts on its target cells by binding to the cognate cysteine-cysteine chemokine receptor 2 (CCR2), a member of the seven-transmembrane G protein-coupled receptor family, which is the main signaling partner of CCL2 (Lee et al., 2009). Recently, the CCL2–CCR2 axis has attracted increasing interest due to its association with tumor progression (Lim et al., 2016). On one hand, CCL2 can be synthesized by metastatic tumor cells and stromal cells in the tumor microenvironment, which is critical for recruiting a subpopulation of CCR2-expressing monocytes or macrophages that enhance the subsequent extravasation of tumor cells (Qian et al., 2011). On the other hand, CCR2 is expressed in various cancer types and regulates CCL2-induced breast cancer cell survival and motility through MAPK- and Smad3-dependent mechanisms (Fang et al., 2012). In addition, CCL2–CCR2 can induce STAT3 activation and epithelial–mesenchymal transition (EMT) of PCa cells (Izumi et al., 2013), and the CCL2–CCR2 axis might promote metastasis of nasopharyngeal carcinoma by activating the ERK1/2–MMP2/9 pathway (Yang et al., 2016). These results support the hypothesis that the CCR2 protein, as a receptor together with its cognate ligand CCL2, promotes cancer metastasis. However, a Kaplan–Meier analysis of disease-specific survival for breast cancer patients stratified by *CCR2* mRNA expression showed that higher expression of *CCR2* mRNA is significantly correlated with longer survival (see Results). Therefore, we postulated that the *CCR2* transcript may perform a different function to its protein in breast cancer progression.

The competing endogenous RNAs (ceRNAs) hypothesis posits that all RNA transcripts can modulate each other's expression by competing for shared microRNAs (miRNA), thus acting as ceRNAs (Cesana et al., 2011; Karreth et al., 2011; Salmena et al., 2011; Sumazin et al., 2011; Tay et al., 2011, 2014). Multiple non-coding RNA species, including small non-coding RNAs, pseudogenes (Zheng et al., 2015), long non-coding RNAs (lncRNAs) (Cesana et al., 2011; Chou et al., 2016; Liu et al., 2013) and circular RNAs (circ RNAs) can possess ceRNA activity. mRNA transcripts may act as tumor suppressors or oncogenes through their ceRNA activity, and this activity may be complementary or even distinct from their protein-coding function (Tay et al., 2014). For example, the ZEB2 protein, promotes the progression of glioma (Li et al., 2016a) and lung cancer (Jiao et al., 2016); however, as a PTEN ceRNA, the *ZEB2* mRNA displays tumor-suppressive properties in melanoma cells (Karreth et al., 2011). To determine the potentially distinct function of the *CCR2* transcript, we examined whether *CCR2* mRNA exerts a tumor-suppressive function in breast cancer through its ceRNA activity.

STARD13 (also called DLC2), a unique Rho GTPase-activating protein (RhoGAP), is underexpressed in some types of cancer and suppresses cytoskeleton reorganization, cell migration and transformation by inhibiting RhoA activity through its RhoGAP domain (Ching et al., 2003; Leung et al., 2005; Lin et al., 2010). Active (GTP-loaded) RhoA binds to and activates Rho-associated coiled-coil-forming kinase 1 (ROCK1).

[1]School of Life Science and Technology, China Pharmaceutical University, Nanjing 210009, People's Republic of China. [2]Jiangsu Key Laboratory of Carcinogenesis and Intervention, China Pharmaceutical University, Nanjing 210009, People's Republic of China. [3]Jiangsu Key Laboratory for Pharmacology and Safety Evaluation of Chinese Materia Medica, School of Pharmacy, Nanjing University of Chinese Medicine, Nanjing 210023, People's Republic of China.

*Authors for correspondence (xitao18@hotmail.com; zhlf@cpu.edu.cn)

J.H., 0000-0002-5608-8430; X.L., 0000-0002-5742-2189; X.G., 0000-0002-7610-0847; Q.G., 0000-0003-2119-1371; C.X., 0000-0003-2259-4471; Z.Z., 0000-0002-9807-4723; Y.X., 0000-0002-2542-127X; T.X., 0000-0001-8065-2639; L.Z., 0000-0002-2183-4974

Received 30 January 2017; Accepted 4 August 2017

Journal of Cell Science (2017) 130, 3399-3413 doi:10.1242/jcs.202127

RhoA-bound ROCK1 activates myosin light chain 2 (MLC2) by phosphorylating it at S19 (denoted $pMLC^{S19}$), increasing the level of $pMLC^{S19}$, which is required to coordinate the formation of stress fibers (Gilkes et al., 2014). Increased formation of the filamentous actin (F-actin) cytoskeleton and enhanced contractility are critical to cell migration (Stricker et al., 2010). miRNAs that target *CCR2* mRNA have not been reported before. Here, TargetScan (www.targetscan.org/) was used to predict the miRNA-binding sites in the *CCR2* 3′-untranslated region (3′UTR), and three microRNA-125b (miR-125b)-binding sites were found to exist in the *CCR2* 3′UTR. Our laboratory has previously shown that miR-125b can promote metastasis of MCF-7 and MDA-MB-231 cells by targeting STARD13 (Tang et al., 2012). Furthermore, our recent study described a STARD13-correlated ceRNA network that possesses a metastasis-suppressive role in breast cancer (Li et al., 2016b). Thus, we deduced that *CCR2* mRNA acts as a tumor suppressor in breast cancer through its ceRNA activity to promote STARD13 expression in a protein-independent but miRNA-dependent way.

This study reveals that the *CCR2* 3′UTR inhibits EMT and modulates STARD13 expression in MDA-MB-231 and MCF-7 cells. The *CCR2* 3′UTR blocked RhoA–ROCK1 signaling, which acts as the downstream effector of STARD13, and thus decreased the phosphorylation of MLC and the formation of F-actin. Taken together, these results delineate a molecular mechanism by which the *CCR2* 3′UTR regulates STARD13 expression and further inactivates the RhoA–ROCK1 pathway, which is required for breast cancer metastasis.

RESULTS

The *CCR2* 3′UTR displays tumor-suppressive properties in breast cancer cells

We first investigated the roles of the *CCR2* 3′UTR in breast cancer development. First, we performed a Kaplan–Meier survival analysis, by using the KM-plotter (Győrffy et al., 2010), which revealed that *CCR2* mRNA level was positively correlated with the longer overall survival (OS) (P=0.0011) (Fig. 1A), distant metastasis-free survival (DMFS) (P=0.018) (Fig. 1B) and relapse-free survival (RFS) ($P=2.9\times10^{-15}$) (Fig. 1C) of breast cancer patients. The results seem to contradict the idea that CCR2 enhances CCL2-induced breast cancer cell survival and motility, which promoted us to explore whether *CCR2* mRNA holds distinct functions other than its protein-coding function. Cell migration was measured in MCF-7 and MDA-MB-231 cells transfected with the *CCR2* 3′UTR or empty vector through wound healing and transwell migration assays. Overexpression of the *CCR2* 3′UTR remarkably decreased the migration of MCF-7 and MDA-MB-231 cells compared with control vector (Fig. 1D,E). Adhesion of tumor cells to extracellular and basement membranes plays a critical role in the initial step in the invasive process (Tang et al., 2012). The adhesion ability of the *CCR2* 3′UTR-transfected cells was decreased in MCF-7 and MDA-MB-231 cells (Fig. 1F). A similar trend was observed in Transwell migration assays (Fig. 1G,H). Additionally, Matrigel invasion chambers were used to examine the role of the *CCR2* 3′UTR towards tumor invasiveness. The invasive ability of the *CCR2* 3′UTR-transfected cells was markedly decreased compared to cells treated with control vector (Fig. 1G,I). In addition, cell cycle analysis showed that no relevant changes were detected upon CCR2 3′UTR ectopic expression in the percentage of cells in G0/G1, G2/M and S phases (Fig. S1A–D). Further cell apoptosis analysis indicated that the *CCR2* 3′UTR overexpression had no significant effect on cell apoptosis (Fig. S1E–H). These results suggest that ectopic expression of the *CCR2* 3′UTR suppresses breast cancer cell metastasis and has no effect on cell cycle progression and apoptosis.

Ectopic expression of the *CCR2* 3′UTR inhibits the EMT process

EMT is the most critical step in tumor metastasis (Biddle and Mackenzie, 2012; Kong et al., 2008). We further sought to determine whether the *CCR2* 3′UTR could reverse the EMT phenotype. As shown in Fig. 2A,B, the ectopic expression of the *CCR2* 3′UTR or STARD13 3′UTR resulted in upregulation of the epithelial marker E-cadherin and downregulation of mesenchymal markers, including N-cadherin, and α-smooth muscle actin (α-SMA, also known as ACTA2) in MCF-7 cells. Furthermore, TGF-β1-induced EMT was used as test model for the effect of *CCR2* 3′UTR overexpression in epithelial MCF-7 cells. At 48 h after TGF-β1 treatment, MCF-7 cells exhibited lower levels of E-cadherin and higher N-cadherin, which was reversed upon *CCR2* 3′UTR overexpression (Fig. 2C). After TGF-β1 treatment, MCF-7 cells underwent a dramatic morphological change, from a cobblestone-like epithelial structure to fibroblastoid spindle-shaped cells. This morphological transition is accompanied by E-cadherin downregulation. However, transfection with the *CCR2* 3′UTR significantly reduced the acquisition of mesenchymal characteristics during the TGF-β1-induced EMT of MCF-7 cells (Fig. 2D). The ectopic expression of the *CCR2* 3′UTR or *STARD13* 3′UTR downregulated mesenchymal markers expression including N-cadherin and vimentin in MDA-MB-231 cells, whereas α-SMA expression was not affected in MDA-MB-231 cells (Fig. 3A,B). Identical results were obtained by immunofluorescence staining analysis (Fig. 3C,D). Taken together, these results demonstrate that the *CCR2* 3′UTR could block the TGF-β1-induced EMT of MCF-7 cells and induce mesenchymal–epithelial transition (MET) in MCF-7 and MDA-MB-231 cells.

The *CCR2* 3′UTR modulates expression of STARD13

Based on the fact that a series of common miRNA response elements (MREs) exist in the 3′UTR of CCR2 and STARD13, we assumed that *CCR2* is a ceRNA candidate for STARD13, which has proven to be a tumor suppressor (Tang et al., 2012). We first examined whether the *CCR2* 3′UTR could modulate STARD13 expression. Ectopic expression of the *CCR2* 3′UTR significantly upregulated the mRNA levels of *CCR2* and *STARD13* in MDA-MB-231 cells (Fig. 4A) and MCF-7 cells (Fig. S2A). Similarly, the *STARD13* 3′UTR also upregulated the mRNA levels of *CCR2* and *STARD13* (Fig. 4B; Fig. S2B). Moreover, STARD13 and CCR2 protein levels were increased in the *CCR2* 3′UTR-transfected (Fig. 4C; Fig. S2C) and *STARD13* 3′UTR-transfected (Fig. 3D; Fig. S2D) breast cancer cells. In contrast, knockdown of *CCR2* reduced *STARD13* mRNA levels and knockdown of STARD13 led to downregulation of *CCR2* mRNA levels in MDA-MB-231 cells (Fig. 4E) and MCF-7 cells (Fig. S2E). Importantly, STARD13 and CCR2 protein levels were reduced following knockdown of *CCR2* or knockdown of *STARD13* in MDA-MB-231 cells (Fig. 4F) and MCF-7 cells (Fig. S2F). These results indicate that CCR2 and STARD13 can regulate each other's expression.

CCR2 is a potential target of miR-125b

To elucidate which miRNA mediates the CCR2–STARD13 crosstalk, we analyzed the common MREs in the 3′UTRs of STARD13 and CCR2. TargetScan 6.2 predicted that CCR2 and STARD13 shared sites for four miRNA families and contained a total of six and nine MREs for these miRNAs, respectively, with

Journal of Cell Science (2017) 130, 3399-3413 doi:10.1242/jcs.202127

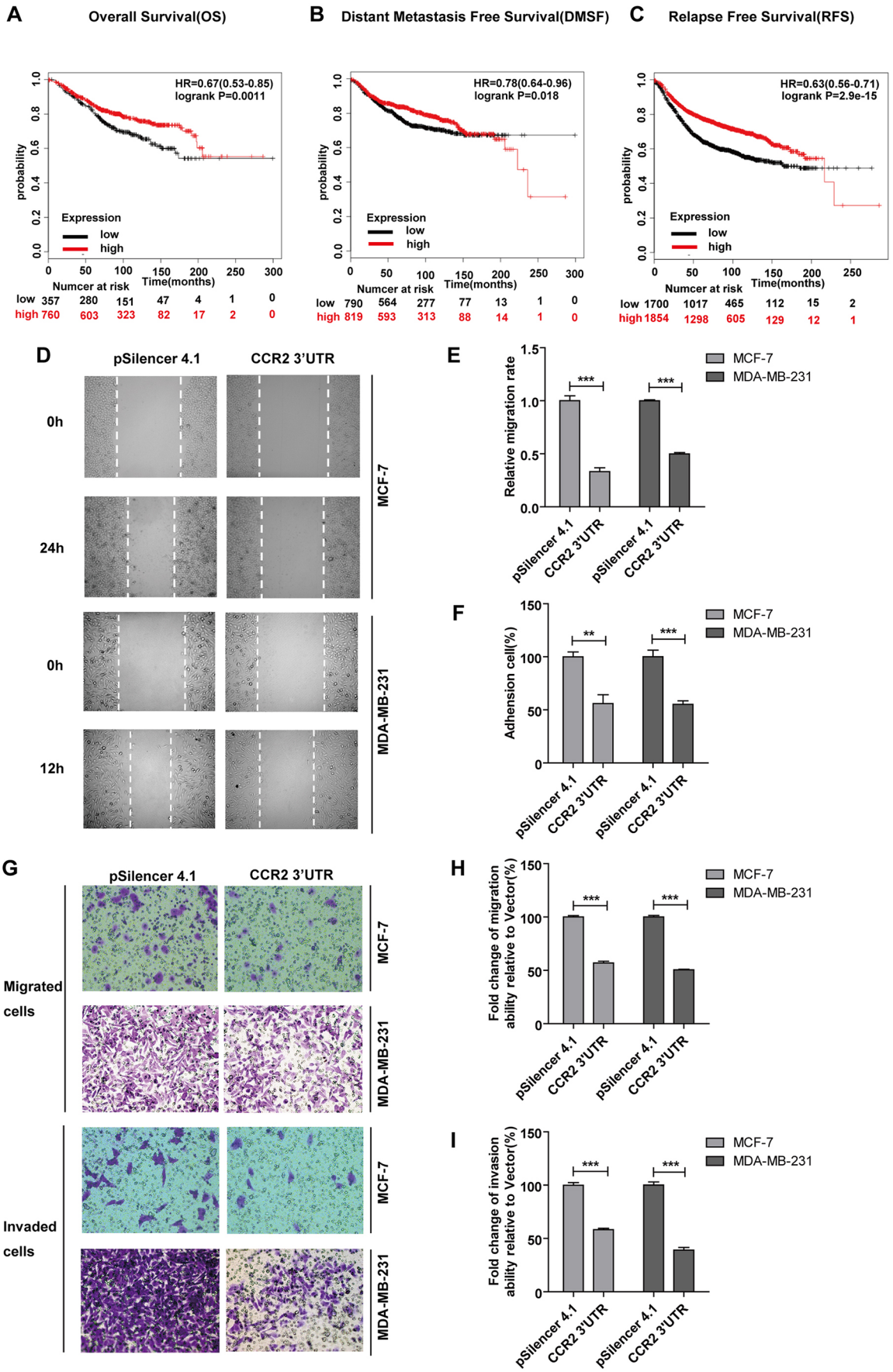

Fig. 1. See next page for legend.

Journal of Cell Science

Journal of Cell Science (2017) 130, 3399-3413 doi:10.1242/jcs.202127

Fig. 1. Effects of the *CCR2* 3′UTR on metastasis in MCF-7 and MDA-MB-231 cells. A good prognosis for breast cancer patients is associated with overexpression of *CCR2* (207794_at). Kaplan–Meier overall survival (A), distant metastasis-free survival (B), relapse-free survival (C) probability for breast cancer patients with high (red) and low (black) *CCR2* gene expression (divided at the median). The hazard ratio (HR) with 95% confidence intervals and logrank P were calculated for the low versus high *CCR2* levels. (D) The cell motility rate was measured with a wound healing assay. Movement of MCF-7 and MDA-MB-231 cells into the wound was shown for the *CCR2* 3′UTR-transfected cells (pSilencer 4.1 harboring the *CCR2* 3′UTR sequence) and pSilencer 4.1-transfected cells. (E) Quantification of the wound healing assay shown in D. (F) Effects of the *CCR2* 3′UTR on adhesion to matrix gel of MCF-7 and MDA-MB-231 cells. (G) Effects of the *CCR2* 3′UTR on vertical migration and cell invasion in MCF-7 and MDA-MB-231 cells as seen from Transwell insert chambers and Matrigel invasion chambers, respectively. (H,I) OD_{570} values of Crystal Violet stain for G. Data are presented as the mean±s.d., n=3. *P<0.05, **P<0.01, ***P<0.001 versus control vector.

miR-125b being one of the shared miRNAs (Fig. 5A). Our previous study has indicated that miR-125b induces breast cancer metastasis by targeting STARD13 directly (Li et al., 2016b), whereas the miR-125b–CCR2 axis needed to be validated. Quantitative real-time RT-PCR (qRT-PCR) analysis confirmed the transfection efficiency of miR-125b mimics and miR-125b inhibitor in MDA-MB-231 (Fig. 5B,C) and MCF-7 cells (Fig. S3A,B). TargetScan 6.2 analysis indicated that STARD13 contains four miR-125b-binding sites on its 3′UTR, and two of these four sites were predicted to be eight nucleotides long (Fig. 5D). To validate whether CCR2 is regulated by miR-125b, TargetScan 6.2 was adopted to predict targets of miR-125b, and the 3′UTR of CCR2 was predicted to contain three complementary sites for the seed region of miR-125b. One of these three sites, starting at nt 169 of the the *CCR2* 3′UTR, was predicted to be eight nucleotides long. *CCR2* 3′UTR fragments containing the wild-type version of this miR-125b target site (CCR2-WT) or with a version with a mutant miR-125b-binding site (CCR2-MUT) were introduced downstream of the luciferase reporter gene in a pMIR-reporter vector (Fig. 5D). CCR2-WT or CCR2-MUT was then co-transfected with miR-125b mimics in MDA-MB-231 and MCF-7 cells (Fig. 5E; Fig. S3C), and we found that the relative luciferase activity of CCR2-WT was attenuated, while the activity of CCR2-MUT was unaffected. To validate the direct binding between miR-125b and the *CCR2* 3′UTR and *STARD13* 3′UTR, we performed an RNA immunoprecipitation (RIP) assay using antibody against Ago2, which is the core component of the RNA-induced silencing complex, to pulldown miRNAs associated with the *CCR2* 3′UTR or *STARD13* 3′UTR. qRT-PCR analysis of results from the RIP assay demonstrated that the amount of miR-125b pulled down (Ago2 enrichment) from MDA-MB-231 cells stably transfected with the *CCR2* 3′UTR [MDA-MB-231$^{(C)}$] or with the *STARD13* 3′UTR [MDA-MB-231$^{(S)}$] was significantly higher than that from MDA-MB-231 cells stably transfected with an empty vector [MDA-MB-231$^{(V)}$] (Fig. 5F). *CCR2* and *STARD13* mRNA levels were significantly decreased or increased with upon transfection with miR-125b mimics or inhibitor, respectively, in MDA-MB-231 (Fig. 5G,H) and MCF-7 cells (Fig. S3D,E). Furthermore, overexpression of miR-125b resulted in a significant reduction in the protein levels of CCR2 and STARD13 (Fig. 5I; Fig. S3F) and knockdown of miR-125b led to an increase in protein levels (Fig. 5J; Fig. S3G). Taken together, these data indicate that *CCR2* is a potential target of miR-125b.

miRNA dependency of the *CCR2*–*STARD13* interaction

To further confirm that *CCR2* acts as a *STARD13* ceRNA, we must confirm that the *CCR2*–*STARD13* interaction is indeed mediated by miRNAs. Thus, siRNA against DICER (also known as DICER1), a miRNA biogenesis protein, was utilized. The efficient knockdown of DICER (siDICER) and the concomitant downregulation of miR-125b have been revealed by our earlier study (Li et al., 2016b). siRNA against *CCR2* (siCCR2) failed to inhibit STARD13 mRNA and protein expression when co-transfected with siDICER, whereas the *CCR2* mRNA level was decreased. Similarly, *STARD13* knockdown diminished the *STARD13* mRNA level but did not affect the CCR2 mRNA and protein level in siDICER-treated cells as compared with negative control (NC) cells (Fig. 6A,B; Fig. S4A,B). Moreover, in the presence of siDICER, the *CCR2* 3′UTR-mediated or *STARD13* 3′UTR-mediated increase of STARD13 and CCR2 protein expression was lost (Fig. 6C,D; Fig. S4C,D). To confirm the pivotal roles of miRNAs in the regulation between CCR2 and STARD13, we performed an RIP assay on Ago2. As shown in Fig. 6E, overexpression of the *CCR2* 3′UTR in MDA-MB-231 cells led to the increased enrichment of Ago2 on the *CCR2* 3′UTR but substantially decreased enrichment on the *STARD13* 3′UTR, and this result suggests that the *CCR2* 3′UTR can compete with *STARD13* transcripts for the Ago2-based miRNA-induced repression complex. Notably, ectopic expression of the *CCR2* 3′UTR with mutation of all three predicted miR-125b-binding sites did significantly upregulate the protein level of CCR2 but caused no significantly change in STARD13 protein level (Fig. 6F). Importantly, a wound healing assay showed that the *CCR2* 3′UTR with mutation of all three predicted miR-125b-binding sites caused no significant decrease in the migration of MDA-MB-231 cells (Fig. 6G). These data indicate that the *CCR2* 3′UTR-mediated regulation of STARD13 is indeed dependent on miRNA and the miR-125b target sites within the *CCR2* 3′UTR, especially, are necessary for the *CCR2* 3′UTR to inhibit the metastasis of breast cancer cells.

The *CCR2* 3′UTR and STARD13 3′UTR suppress RhoA activity, MLC phosphorylation and formation of stress fibers

To study whether the *CCR2* 3′UTR could regulate the downstream signals of STARD13, immunofluorescence staining of filamentous actin (F-actin) with Rhodamine-labeled phalloidin was performed, and this revealed that stress fiber formation was markedly inhibited in the *CCR2* 3′UTR- and *STARD13* 3′UTR-transfected cells (Fig. 7A; Fig. S5A). Additionally, the levels of pMLC^{S19} were decreased significantly in the *CCR2* 3′UTR-transfected (Fig. 7B; Fig. S5B) and STARD13 3′UTR-transfected (Fig. 7C; Fig. S5C) cells. To further determine whether RhoA or ROCK1 was involved in the *CCR2* 3′UTR- or *STARD13* 3′UTR-mediated inhibition of MLC phosphorylation, qRT-PCR and western blot analyses were performed, and revealed that the *CCR2* 3′UTR and *STARD13* 3′UTR had no effect on expression of RhoA and ROCK1 in MDA-MB-231 cells (Fig. 7D–G) and in MCF-7 cells (Fig. S5D–G). Furthermore, a G-LISA RhoA activation assay revealed that *CCR2* 3′UTR-transfected cells had a lower basal level of RhoA activity (Fig. 7H). In summary, these data indicate that the *CCR2* 3′UTR and *STARD13* 3′UTR inhibit the formation of F-actin and MLC phosphorylation through regulating RhoA activity rather than by altering RhoA and ROCK1 expression in human breast cancer cells.

The decreased formation of stress fibers and MLC phosphorylation mediated by *CCR2* 3′UTR is dependent on STARD13

We observed that the *CCR2* 3′UTR could inhibit formation of F-actin and MLC phosphorylation. To further ascertain whether these observed effects are dependent upon STARD13 expression, we

Journal of Cell Science (2017) 130, 3399-3413 doi:10.1242/jcs.202127

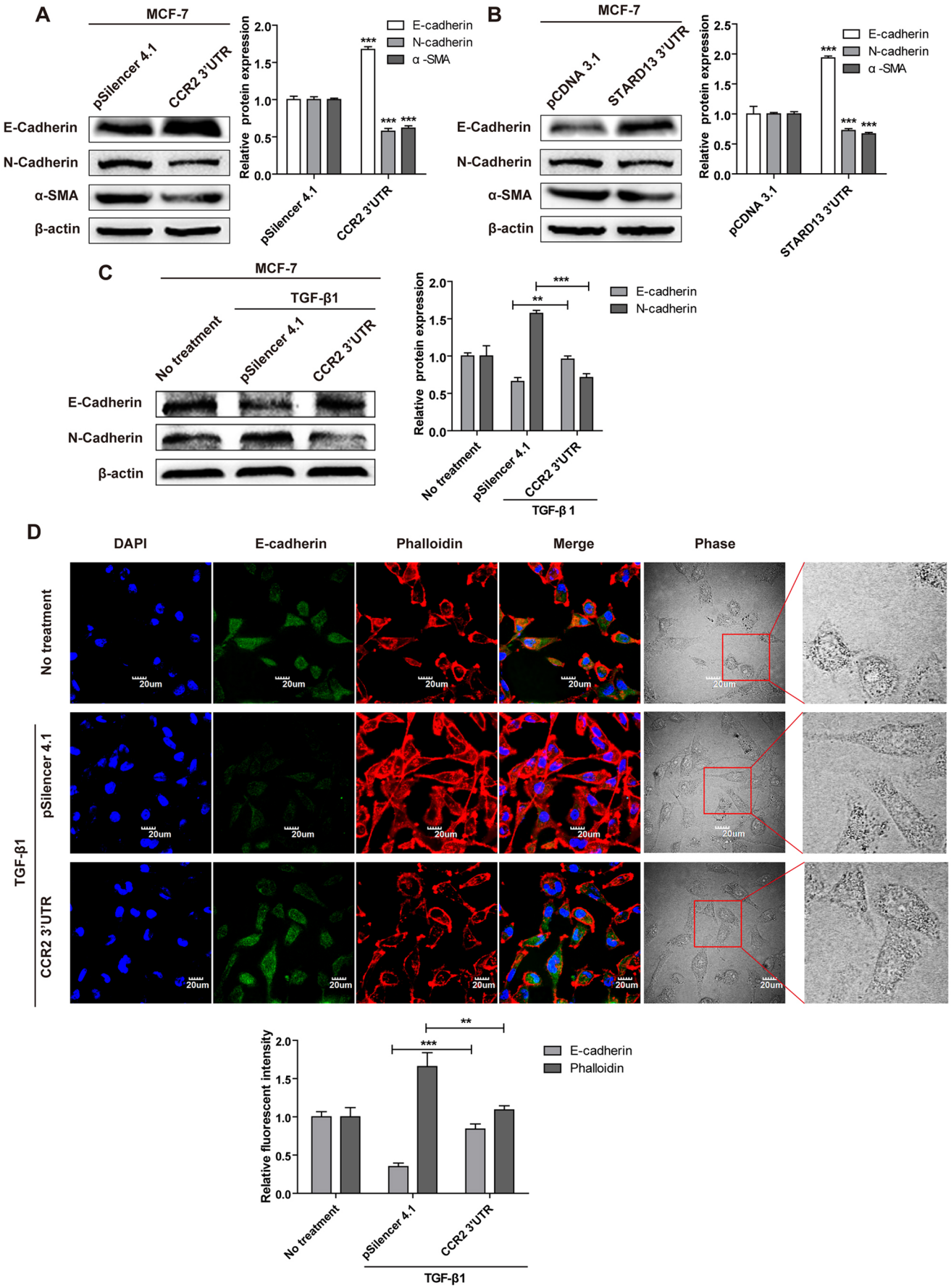

Fig. 2. See next page for legend.

Journal of Cell Science (2017) 130, 3399-3413 doi:10.1242/jcs.202127

Fig. 2. Ectopic expression of the *CCR2* 3′UTR or *STARD13* 3′UTR hinders EMT of MCF-7 cells. (A) Western blot showing effects of the *CCR2* 3′UTR on the expression of E-cadherin, N-cadherin and α-SMA in MCF-7 cells (left panel). Right panel, quantification of the protein expression. (B) Western blot showing effects of *STARD13* 3′UTR on the expression of E-cadherin, N-cadherin and α-SMA in MCF-7 cells (left panel). Right panel, quantification of the protein expression. (C) The expression of E-cadherin and N-cadherin were detected by western blotting in MCF-7 cells transfected with the *CCR2* 3′ UTR and then treated with TGF-β1 for 48 h (left panel). Right panel, quantification of E-cadherin and N-cadherin expression. (D) Immunofluorescence staining of E-cadherin and immunofluorescence staining of filamentous actin (F-actin) with Rhodamine-labeled phalloidin in MCF-7 cells untreated or treated with TGF-β1 after being transfected with negative control pSilencer 4.1 or the *CCR2* 3′UTR. Scale bars: 20 µm. Phase-contrast images are also shown. Data are presented as the mean±s.d., n=3. *P<0.05, **P<0.01, ***P<0.001 versus control vectors.

undertook immunofluorescence staining of F-actin, and showed that siRNA against STARD13 (siSTARD13) could reverse the *CCR2* 3′ UTR-mediated inhibition on stress fiber formation (Fig. 7I; Fig. S5H), suggesting that the *CCR2* 3′UTR induces cell migration via STARD13. Furthermore, blocking STARD13 expression with siSTARD13 abolished the *CCR2* 3′UTR-induced decrease of $pMLC^{S19}$ in MDA-MB-231 (Fig. 7J) and MCF-7 cells (Fig. S5I). Taken together, these results demonstrate that the decreased MLC phosphorylation and formation of stress fibers induced by the *CCR2* 3′UTR are dependent on STARD13.

The *CCR2* 3′UTR inhibits breast cancer metastasis in a xenograft model

The antitumor function of the *CCR2* 3′UTR in breast cancer was further confirmed *in vivo*. qRT-PCR analysis demonstrated the efficient overexpression of the *CCR2* 3′UTR in stably transfected cells (Fig. 8A). MDA-MB-$231^{(C)}$ cells expressed more CCR2 and STARD13 protein (Fig. S6A) and less pMLC protein (Fig. S6B) than MDA-MB-$231^{(V)}$ cells. The morphology in the MDA-MB-$231^{(C)}$ cells, which are stably transfected with the *CCR2* 3′UTR, was round in shape, rather than the angular and spindular shape seen in MDA-MB-$231^{(V)}$ cells, and the stress fiber formation was inhibited in the MDA-MB-$231^{(C)}$ cells (Fig. S6C). Additionally, MDA-MB-231 cells stably transfected with the *CCR2* 3′UTR had a significantly decreased level of cell migration (Fig. S6D). We intravenously transplanted MDA-MB-$231^{(V)}$ or MDA-MB-$231^{(C)}$ into nude mice. As seen in Fig. 8B, micro-computed tomography (micro-CT) analysis revealed that the *CCR2* 3′UTR overexpression strikingly decreased the lung metastasis of MDA-MB-231 cells *in vivo*. The Carestream noninvasive optical imaging system was used for whole-animal imaging, and animals injected with cells stably transfected with the *CCR2* 3′UTR showed a reduced metastasis signals in ventral views (Fig. 8C). Notably, the *CCR2* 3′UTR suppressed pulmonary metastasis of MDA-MB-231 cells, as shown by the bioluminescence of the excised tissues (Fig. 8D). Again, histopathological analysis confirmed the inhibitory effect of the *CCR2* 3′UTR on pulmonary metastasis (Fig. 8E). Our *in vivo* data further strengthen the finding that the *CCR2* 3′UTR has an anti-metastatic effect in breast cancer.

DISCUSSION

The present study shows that the *CCR2* 3′UTR induces a miRNA-dependent increase of STARD13 expression, leading to downstream pathway inactivation that is manifested by the decrease of RhoA activation, actin polymerization and MLC phosphorylation, and thus suppresses breast cancer metastasis (Fig. S7).

CCR2 is viewed as receptor of CCL2, and the CCL2–CCR2 axis has been shown to play crucial roles in cancer metastasis. Targeting this signaling pair is considered as a therapeutic intervention. However, therapeutics obstructing this chemokine receptor pair have displayed disappointing results in the clinic (Lim et al., 2016). Our analyses found that breast cancer patients with higher *CCR2* mRNA expression have a longer overall survival, distant metastasis-free survival and a longer relapse-free survival. This suggests that high *CCR2* mRNA is a marker for good prognosis in breast cancer. We analyzed the inconsistency between results found for *CCR2* transcript and CCR2 protein for the first time, and demonstrated that CCR2 mRNA and protein exert different biological effects. The ceRNA hypothesis was used to explain the molecular mechanism of *CCR2* mRNA action. The ceRNA hypothesis provides a new angle for studying the multilayered complexity of genes. Although it has been proposed that ceRNA regulation is rare and can only exist in certain regimes of target and miRNA abundance (Bosson et al., 2014; Denzler et al., 2014, 2016), the discovery of functional ceRNA regulation in diverse cancer progression by multiple independent groups suggests that ceRNA may represent a widespread layer of gene regulation (Fang et al., 2013; Kumar et al., 2014; Tay et al., 2014). In order to reveal the function of a gene, we should integrate the classic ‘protein dimension’ with an additional ‘ceRNA dimension’ (Karreth et al., 2011).

It has recently been reported that CCR2 knockdown in 4T1 and MCF-7 cells can block CCL2-induced wound closure (Fang et al., 2012). In contrast, we proved that overexpression of the *CCR2* 3′ UTR suppressed breast cancer cells migration and invasion. One possible explanation for this discrepancy is that cells were not stimulated with CCL2 in our experiments. In addition, the *CCR2* 3′ UTR had an influence on biomarkers of EMT, which indicated that the *CCR2* 3′UTR could affect breast cancer cell metastasis through suppressing the EMT process. Notably, a nude mice xenograft model verified the inhibitory role of the *CCR2* 3′UTR on breast cancer metastasis *in vivo*.

Our previous studies have implicated STARD13 as a metastatic suppressor in MCF-7 and MDA-MB-231 cells *in vitro* and *in vivo*, and miR-125b can negatively regulate the expression of STARD13 by targeting STARD13 directly (Li et al., 2016b; Tang et al., 2012). Although a series of experiments were performed to validate that CCR2 and STARD13 could regulate each other’s expression, the ceRNA crosstalk is complex and multi-level. We have to point out that this study did not concentrate some additional considerations of ceRNA activity, such as the abundance of key players, potential interplay with RNA-binding proteins (RBPs) and RNA editing, which may have effects on ceRNA crosstalk (Tay et al., 2014). Analyzing the miRNA-binding sites located in the *CCR2* 3′UTR has suggested that numerous miRNAs could bind with the *CCR2* 3′UTR. The change in the expression level of CCR2 could affect the level of these potential CCR2-binding miRNAs, which in turn could affect the level of other targets. In addition to the direct interactions through shared miRNAs, secondary indirect interactions may also have a profound effect on ceRNA regulation. Originally, ceRNAs were defined as target RNAs of miRNAs that cross talk via competition over binding to their common miRNA regulators. However, by the same logic, miRNAs that share targets compete over binding to their common targets and therefore also exhibit ceRNA-like behavior. Thus, the term ceRNA should be expanded to encompass both types of competing elements. This suggests that perturbation effects could propagate in the network through a cascade of coregulated target RNAs and miRNAs that share targets, leading

Journal of Cell Science (2017) 130, 3399-3413 doi:10.1242/jcs.202127

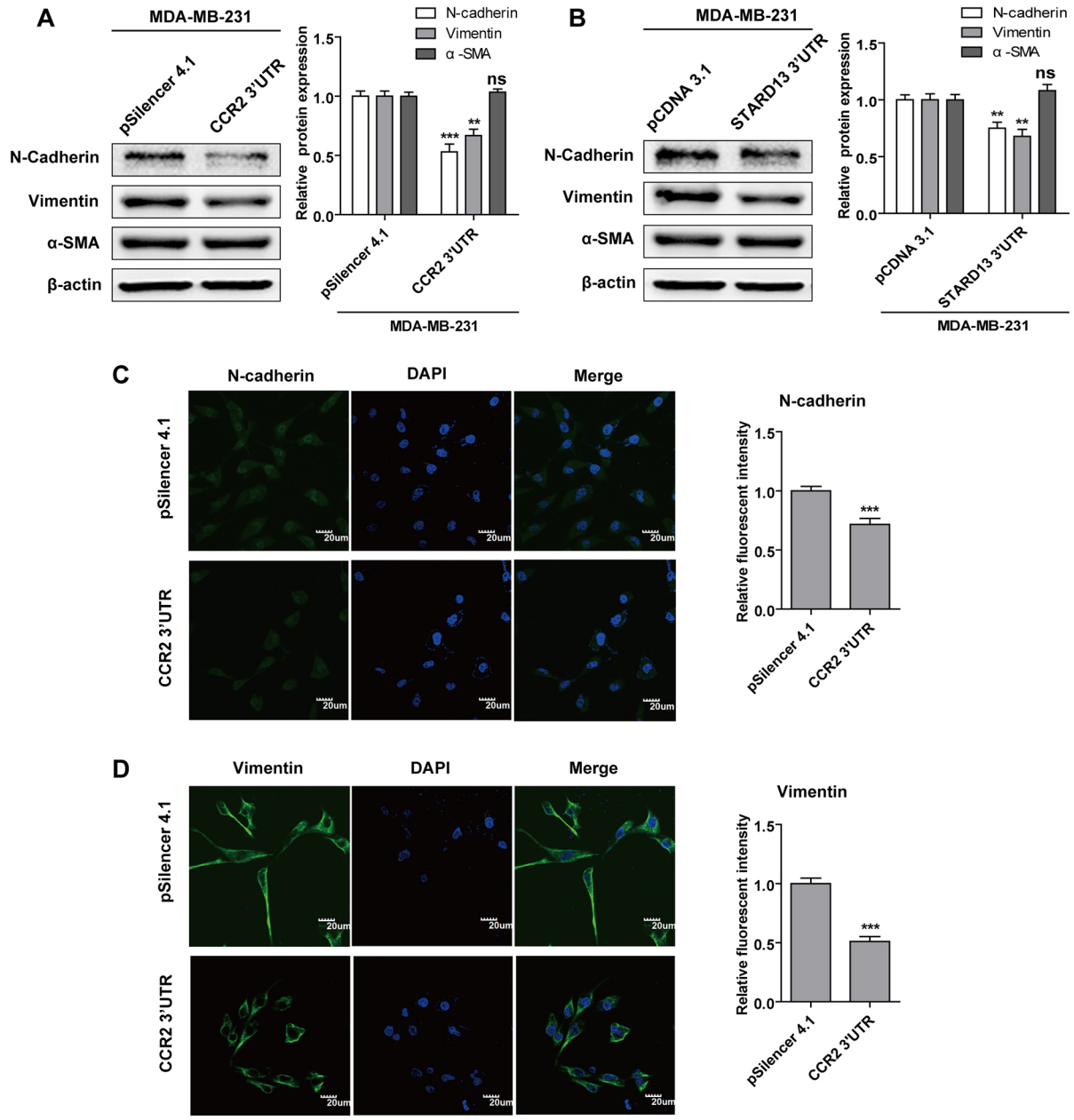

Fig. 3. Ectopic expression of the *CCR2* 3′UTR or *STARD13* 3′UTR leads to the alteration of EMT markers of MDA-MB-231 cells. (A) Western blot showing effects of the *CCR2* 3′UTR on the expressions of N-cadherin, vimentin and α-SMA in MDA-MB-231 cells (left panel). Right panel, quantification of the protein expression. (B) Western blot showing effects of the *STARD13* 3′UTR on the expression of N-cadherin, vimentin and α-SMA in MDA-MB-231 cells (left panel). Right panel, quantification of the protein expression. (C,D) Immunofluorescence staining of N-cadherin (C) and vimentin (D) in MDA-MB-231 cells after being transfected with negative control pSilencer 4.1 or the *CCR2* 3′UTR. Scale bars: 20 µm. Data are presented as the mean±s.d., n=3. *P<0.05, **P<0.01, ***P<0.001 versus control vector.

to mutual effects between distant components in the network, i.e. distant ceRNAs (Nitzan et al., 2014). There is increasing evidence confirming that ceRNAs crosstalk in large interconnected networks (Tay et al., 2014). Further studies are needed to accurately identify metastasis-related miRNA and mRNAs in the CCR2-correlated ceRNA network.

TargetScan was employed because this algorithm considers MRE conservation between mammals, TargetScan predicted that CCR2 and STARD13 are targets for four shared miRNA families; among them, the number of miR-125b MREs in the *CCR2* 3′UTR and STARD13 3′UTR was more than that found for the other miRNAs, therefore miR-125b was used as a model to explore the CCR2–STARD13 interaction. As expected, our results showed that miR-125b can inhibit CCR2 expression. siDICER was used to present an ideal system to evaluate miRNA-dependent effects, and the results showed that the CCR2–STARD13 is interaction is an miRNA-mediated and MRE-dependent regulation. It was specifically found that miR-125b target sites within the *CCR2* 3′ UTR were necessary for the CCR2–STARD13 interaction. Overexpression of the *CCR2* 3′UTR caused a different fold-increase in the CCR2 or STARD13 mRNA compared to that of the protein; a possible explanation for this is that, in contrast to the transcription process, the translation process is regulated by other mechanisms such as phosphorylation, acetylation, ubiquitylation

Journal of Cell Science (2017) 130, 3399-3413 doi:10.1242/jcs.202127

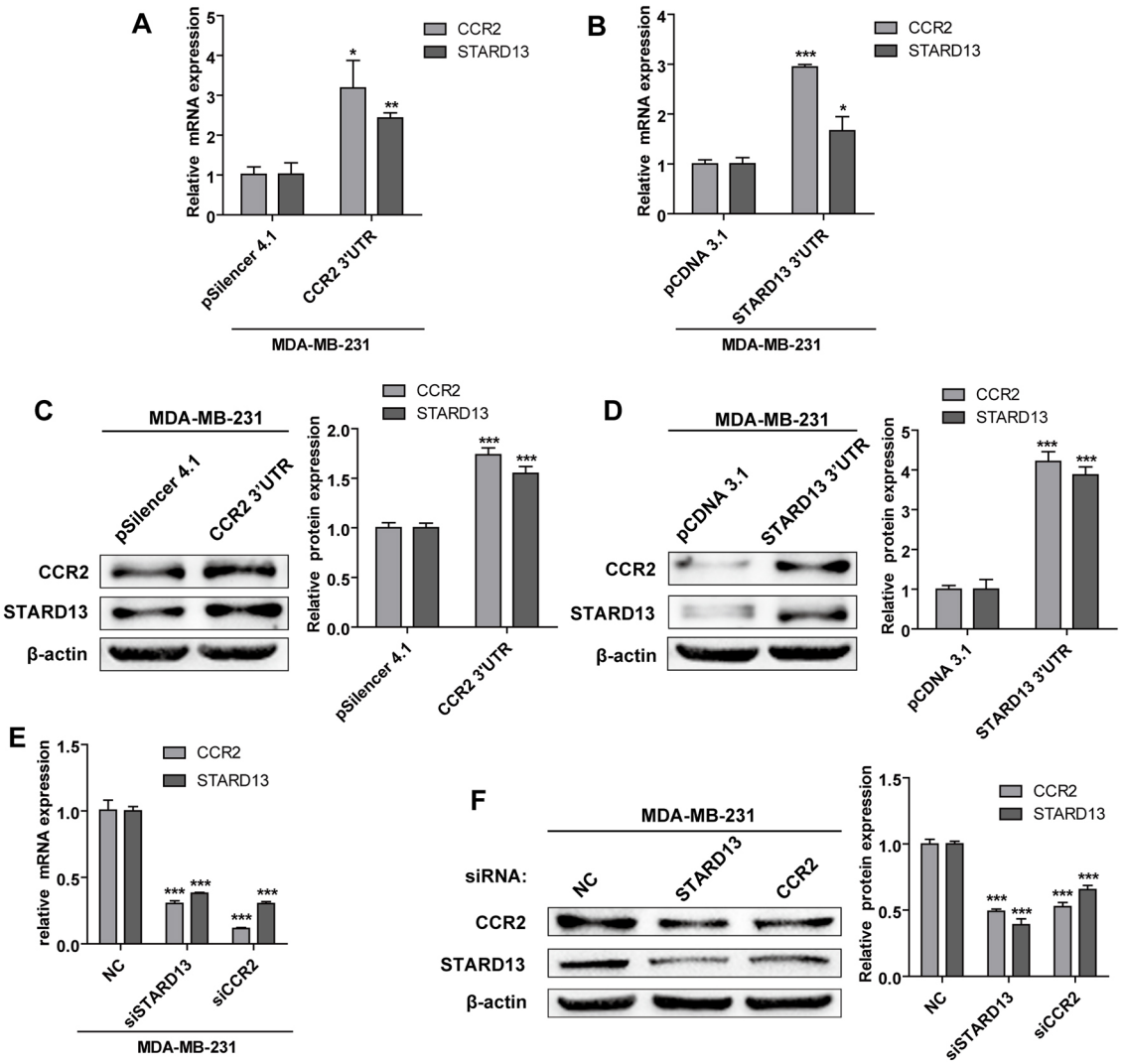

Fig. 4. Expression of the *CCR2* 3′UTR increases STARD13 expression and *CCR2* knockdown decreases STARD13 expression. (A,B) Overexpression of the *CCR2* 3′UTR (A) or *STARD13* 3′UTR (B) increased *CCR2* and *STARD13* mRNA levels in MDA-MB-231 cells as shown by qRT-PCR analysis for expressions of *CCR2* and *STARD13*. (C,D) Overexpression of the *CCR2* 3′UTR (left panel of C) or *STARD13* 3′UTR (left panel of D) increased CCR2 and STARD13 protein levels in MDA-MB-231 cells as shown by western blot analysis for CCR2 and STARD13 expression. β-actin is a shown as a loading control. The right panels of C and D show a quantification of CCR2 and STARD13 expression. (E) *CCR2* and *STARD13* mRNA expression is efficiently reduced following treatment of MDA-MB-231 cells with STARD13 (siSTARD13) or CCR2 siRNA (siCCR2) as shown by qRT-PCR analysis for expression of *CCR2* and *STARD13*. (F) *STARD13* or *CCR2* knockdown decreased CCR2 and STARD13 protein levels in MDA-MB-231 cells (left panel) as shown by western blot analysis for CCR2 and STARD13 expression. β-actin is shown as a loading control. The right panel shows a quantification of CCR2 and STARD13 expression. Data are presented as the mean±s.d., n=3. *P<0.05, **P<0.01, ***P<0.001 versus control vector. NC, negative control siRNA.

and proteolysis of core components of the translation machinery (de Sousa Abreu et al., 2009). In addition, and more remarkably, TargetScan list two transcript variants of *CCR2*, only one of which contains miR-125b target sites; the 3′UTR sequence we study belongs to CCR2 (ENSG00000121807.5), which TargetScan considers as the less-prevalent transcript; therefore, considerations such as the percentage of the transcript variants to the function of CCR2 and the mutual regulation of the two transcript variants still need further study. Importantly, further experiments should focus on whether there a particular 3′UTR variant that can repress *CCR2* translation, while stabilizing the 3′UTR allowing it to act as a ceRNA, and whether there are cancer-specific regulatory pathways that promote CCR2 protein degradation, while stabilizing the mRNA.

As STARD13 is a major antagonist of RhoA–ROCK1 signaling, we examined whether CCR2 can inactivate this pathway via acting as a *STARD13* ceRNA. Intriguingly, the *CCR2* 3′UTR inhibits RhoA activity rather than the expression of total RhoA and ROCK1. These findings rule out the possibility of a direct action between the *CCR2* 3′UTR and RhoA, and proved that the *CCR2* 3′UTR-mediated inhibition of the RhoA activity is dependent on a RhoGAP-containing protein instead acting through another mechanism. RhoA and ROCK1 expression can phosphorylate and inhibit myosin phosphatase (MYPT) and activate focal adhesion kinase (FAK, also known as PTK2) in hypoxic breast cancer cells (Gilkes et al., 2014). Further research is needed to confirm whether the phosphorylation of MYPT and FAK will be affected by the *CCR2* 3′UTR. The *CCR2* 3′UTR-induced decrease of $pMLC^{S19}$ and inhibition of stress fiber formation were abolished by STARD13 siRNA, indicating that STARD13 acted as a downstream effector of the *CCR2* 3′UTR. Since our previous

Journal of Cell Science (2017) 130, 3399-3413 doi:10.1242/jcs.202127

A

Common miRNAs	Number of MREs in CCR2	Number of MREs in STARD13
miR-125a-5p/125b-5p/351/670/4319	3	4
miR-204/204b/211	1	3
miR-25/32/92abc/363/363-3p/367	1	1
miR-23abc/23b-3p	1	1

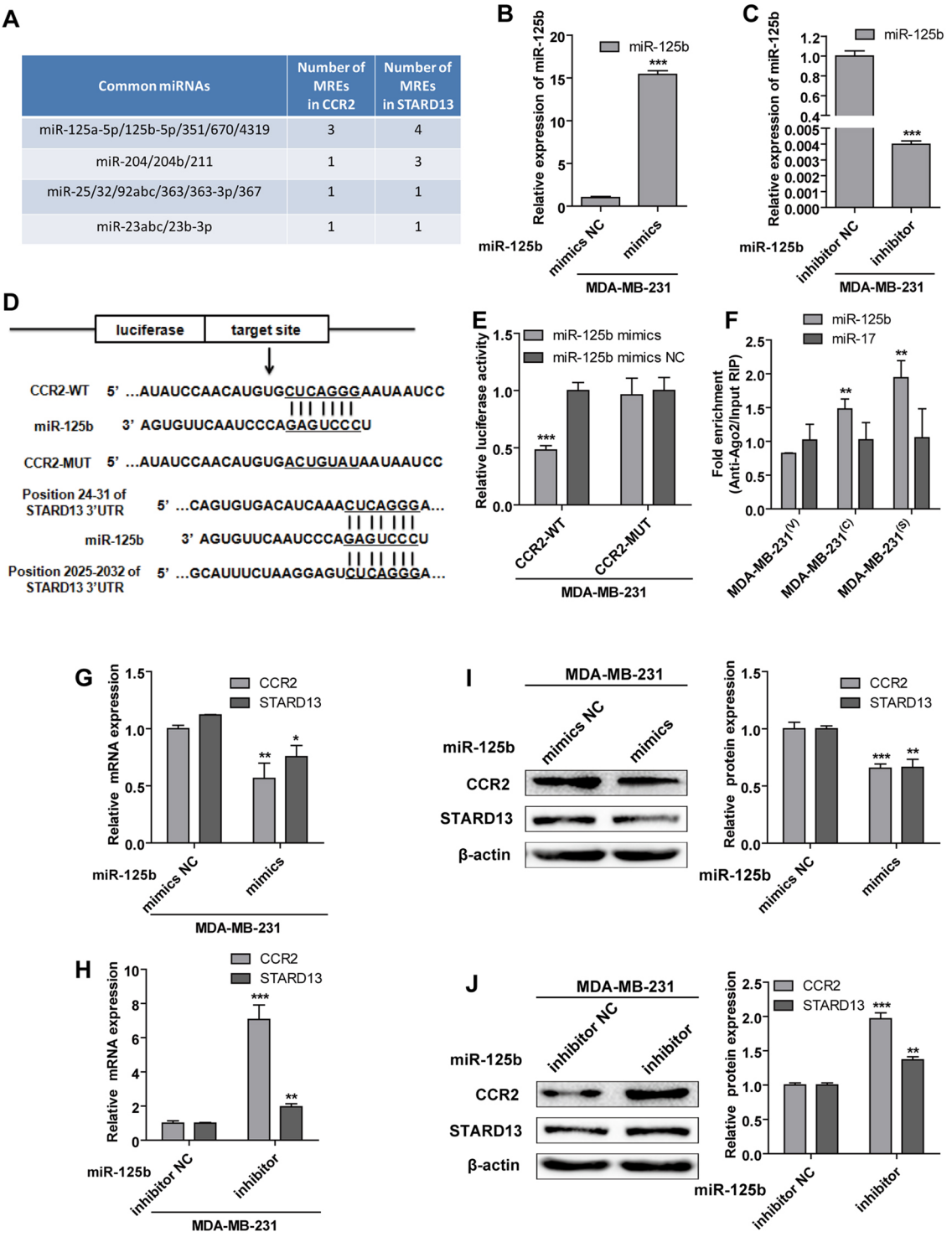

Fig. 5. miR-125b regulates CCR2 and STARD13 expression. (A) miRNA response elements (MREs) shared by CCR2 and STARD13. The 3′UTR of *CCR2* and *STARD13* have binding sites for four miRNA families in common, and this table depicts the number of sites for each miRNA. (B,C) The transfection efficiency of miR-125b mimics (B) and miR-125b inhibitor (C) was confirmed by qRT-PCR in MDA-MB-231 cells. Data are presented as the mean±s.d., n=3. *P<0.05, **P<0.01, ***P<0.001 versus mimics NC or inhibitor NC. (D) Sketch of the construction of CCR2-WT or CCR2-MUT vectors. Potential binding sites for miR-125b on the *STARD13* 3′UTR are shown (underlined). (E) After transfection, a luciferase reporter assay confirmed the direct binding between miR-125b and *CCR2* in MDA-MB-231 cells. Luciferase activity in cells was measured and normalized to β-gal activity. Data are presented as the mean±s.d., n=3. *P<0.05, **P<0.01, ***P<0.001 versus mimics NC. (F) RIP assay followed by miRNA qRT-PCR to detect the association of miR-125b with the *CCR2* 3′UTR or *STARD13* 3′UTR. miR-17 was used as a negative control since there is no binding site for miR-17 on the *CCR2* 3′UTR or *STARD13* 3′UTR. Data are presented as the mean±s.d., n=3. *P<0.05, **P<0.01, ***P<0.001 versus MDA-MB-231$^{(V)}$. (G) miR-125b mimics reduced the mRNA levels of *CCR2* and *STARD13* in MDA-MB-231 cells. (H) miR-125b inhibitor increased the mRNA levels of *CCR2* and *STARD13* in MDA-MB-231 cells. (I,J) Western blot analysis of CCR2 and STARD13 expression in MDA-MB-231 cells treated with miR-125b mimics (left panel of I) or miR-125b inhibitor (left panel of J). β-actin expression is shown as a loading control. The right panels of I and J show a quantification of the protein expression. Data are presented as the mean±s.d., n=3. *P<0.05, **P<0.01, ***P<0.001 versus mimics NC or inhibitor NC.

Journal of Cell Science (2017) 130, 3399-3413 doi:10.1242/jcs.202127

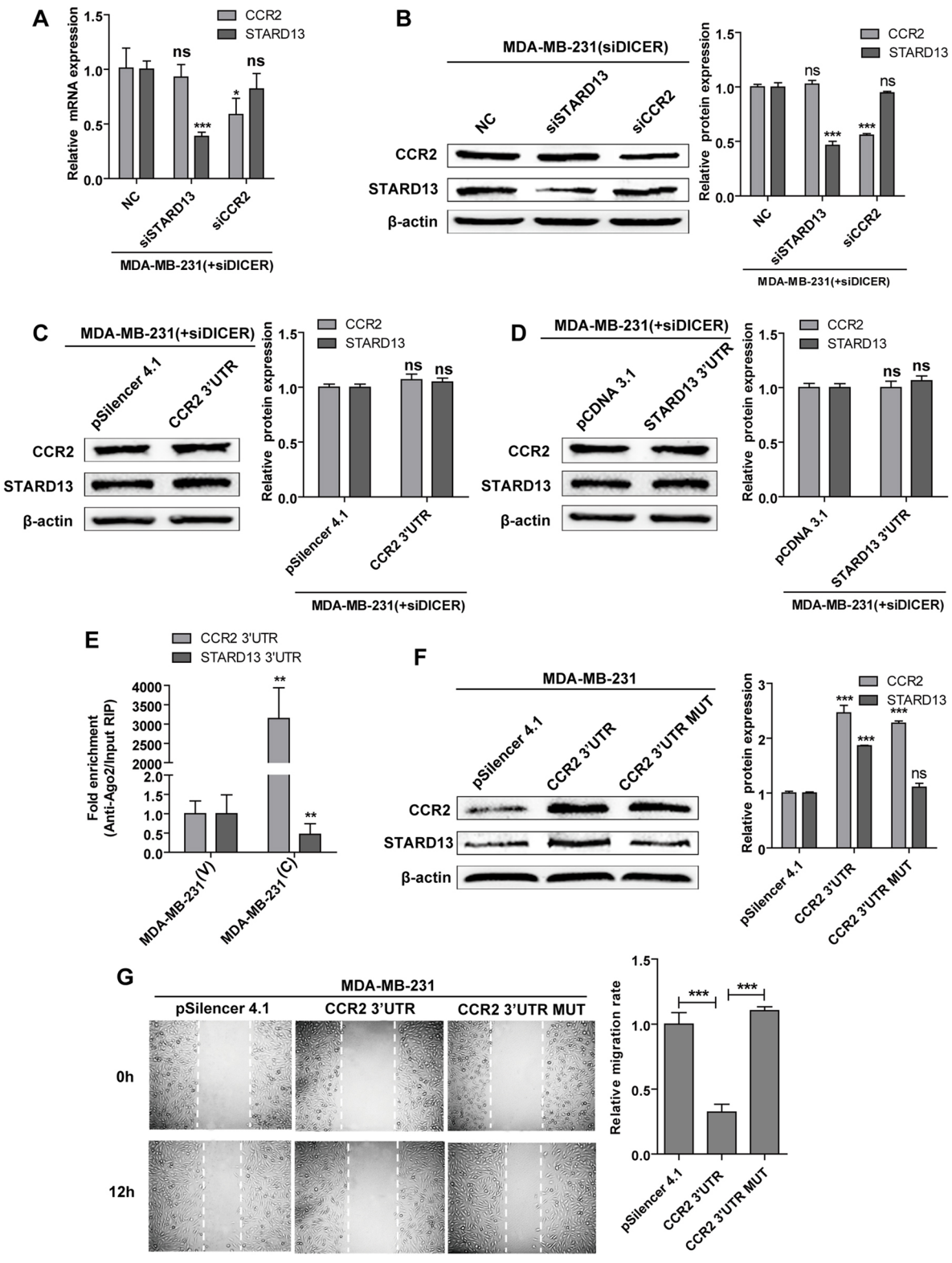

Fig. 6. Regulation of STARD13 by CCR2 is miRNA dependent. (A,B) The mRNA (A) and protein (B) expressions of STARD13 and CCR2 was examined by qRT-PCR analysis or western blot analyses for cells with co-transfection of siCCR2 with siDICER. Data are presented as the mean±s.d., *n*=3. **P*<0.05; ***P*<0.01; ****P*<0.001; ns, not significant versus NC. (C,D) Western analyses were used to detect CCR2 and STARD13 protein expression in response to the overexpression of *CCR2* 3′UTR (left panel of C) and *STARD13* 3′UTR (left panel of D) in siDICER-treated MDA-MB-231 cells. Right panels of C and D show a quantification of protein expression. (E) RIP assay followed by qRT-PCR to detect the enrichment of Ago2 on the *CCR2* 3′UTR and *STARD13* 3′UTR in MDA-MB-231$^{(V)}$ cells and in MDA-MB-231$^{(C)}$ cells. (F) Western blot analyses were performed to evaluate CCR2 and STARD13 protein expression in response to the *CCR2* 3′UTR or the *CCR2* 3′UTR MUT in MDA-MB-231cells (left panel). The right panel shows a quantification of protein expression. (G) The cell motility rate was measured with a wound healing assay; movement of MDA-MB-231 cells into the wound is indicated for pSilencer 4.1, the *CCR2* 3′UTR and the *CCR2* 3′UTR MUT. Data are presented as the mean±s.d., *n*=3. **P*<0.05; ***P*<0.01; ****P*<0.001; ns, not significant versus control vector.

Journal of Cell Science (2017) 130, 3399-3413 doi:10.1242/jcs.202127

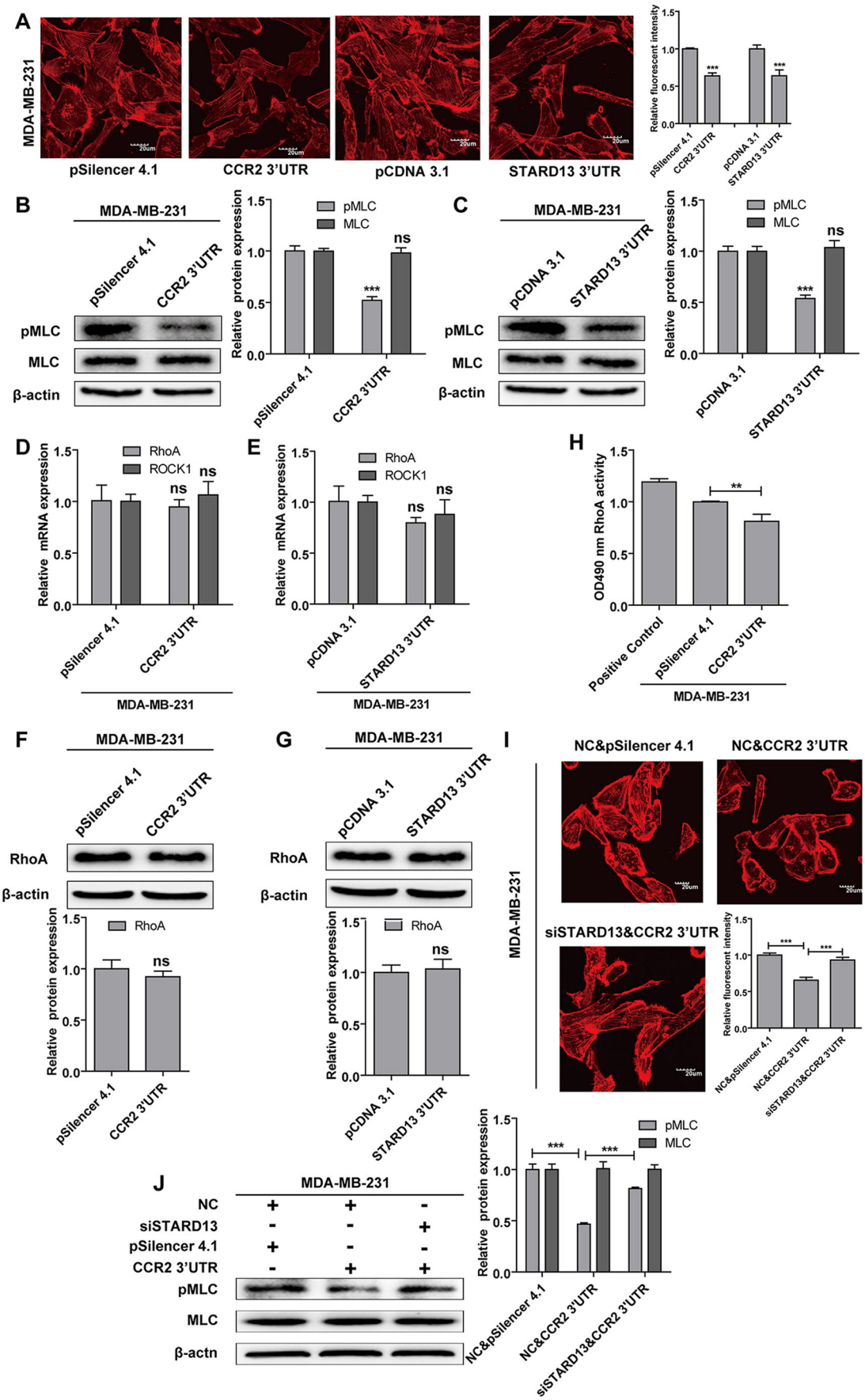

Fig. 7. See next page for legend.

Journal of Cell Science (2017) 130, 3399-3413 doi:10.1242/jcs.202127

Fig. 7. The *CCR2* 3′UTR inhibits formation of F-actin stress fibers, RhoA activity and MLC phosphorylation. (A) MDA-MB-231 cells transfected as indicated were stained with Rhodamine-labeled phalloidin to detect F-actin stress fibers. Scale bars: 20 µm. (B,C) Western blot analysis was used to detect $pMLC^{S19}$ protein in response to overexpression of the *CCR2* 3′UTR (left panel of B) and STARD13 3′UTR (left panel of C) in MDA-MB-231 cells. The right panels of B and C show a quantification of $pMLC^{S19}$ and MLC protein. (D,E) qRT-PCR was performed to quantify *RhoA* and *ROCK1* mRNA levels in MDA-MB-231 cells transfected as indicated. (F,G) Western blotting was performed to examine total RhoA protein level in response to overexpression of the *CCR2* 3′UTR (upper panel of F) and *STARD13* 3′UTR (upper panel of G) in MDA-MB-231 cells. The lower panel of F and G show a quantification of RhoA protein. Data are presented as the mean±s.d., n=3. *P<0.05, **P<0.01, ***P<0.001 vesus control vector. ns indicates no significant differences from control vector (pSilencer 4.1 or pCDNA 3.1). (H) RhoA activation was measured by G-LISA. Absorbance was read at 490 nm. Data are presented as the mean±s.d., n=3. *P<0.05, **P<0.01, ***P<0.001 versus control vector (pSilencer 4.1). (I) MDA-MB-231 cells were transfected with siSTARD13 or NC siRNA in the presence or absence of overexpression the *CCR2* 3′UTR and stained with Rhodamine-labeled phalloidin. An immunofluorescence assay confirmed that siSTARD13 inhibited the *CCR2* 3′UTR-induced downregulation of F-actin. Scale bars: 20 µm. (J) siSTARD13 inhibited the *CCR2* 3′UTR-induced downregulation of phosphorylation of MLC protein in MDA-MB-231 cells (left panel). The right panel of J shows a quantification of $pMLCS^{19}$ and MLC protein. Data were presented as the mean±s.d., n=3. *P<0.05, **P<0.01, ***P<0.001 versus NC and pSilencer 4.1, or siSTARD13 and *CCR2* 3′UTR.

study has confirmed that a STARD13-correlated ceRNA network can inhibit breast cancer metastasis (Li et al., 2016b), further investigation should be carried out to confirm the regulation between the CCR2 and STARD13-correlated ceRNA network.

Although several clinical trials targeting the CCL2–CCR2 signaling axis have been established, the CCL2–CCR2 signaling network is undeniably far more complex than that suggested by the current researches (Lim et al., 2016). There is still has a long way to go before CCL2- or CCR2-targeted therapies can be set up successfully. The non-coding function of mRNA might create functional complexity and diversification in both physiological and pathological conditions, and the unappreciated genetic dimension should be considered when designing treatment strategy.

MATERIALS AND METHODS

Cell lines and culture

Human breast cancer cell lines MCF-7 and MDA-MB-231 were obtained from the ATCC (Manassas, VA) and maintained in high-glucose Dulbecco's modified Eagle's medium (DMEM) and L15 medium (Gibco), respectively. Both media were supplemented with 10% fetal bovine serum (FBS) (Gibco), 80 U/ml penicillin and 0.08 mg/ml streptomycin, and cells were incubated at 5% CO_2 at 37°C. L15 medium with 0.6 µg/ml puromycin was used to incubate MDA-MB-231$^{(C)}$ cells (stably transfected with the *CCR2* 3′UTR), MDA-MB-231$^{(V)}$ cells (stably transfected with an empty vector) and MDA-MB-231$^{(S)}$ (stably transfected with the *STARD13* 3′UTR).

MicroRNA, siRNA, plasmids and transfection

miRNA mimics and inhibitor, negative control (NC) mimics and inhibitor, siRNA and NC siRNA were synthesized by Biomics Biotechnology, China. Sequences of siRNA were: CCR2 siRNA (sense strand, 5′-CAUCAAUCCC AUCAUCUAU-3′), STARD13 siRNA (sense strand, 5′-CACCUUUCCAU CUCCUAAU-3′), DICER siRNA (sense strand, 5′-AAGGCUUACCUU CUCCAGGCU-3′). The *CCR2* 3′UTR (NM_001123396.1) and *STARD13* 3′UTR were cloned into the pSilencer 4.1 vector (Ambion) and the pCDNA 3.1 vector (Invitrogen), respectively, and the constructs were verified by DNA sequencing. The recombinant plasmids were denoted the *CCR2* 3′ UTR and *STARD13* 3′UTR, respectively. The *CCR2* 3′UTR with mutation of all three predicted miR-125b-binding sites were cloned into the pSilencer 4.1 vector and was denoted the *CCR2* 3′UTR MUT. Lipofectamine 2000 Reagent (Invitrogen) was used for the miRNA mimics and inhibitor, mimics NC, inhibitor NC, siRNA, NC and plasmid transfection. At 48 h after transfection, the mRNA expression was assessed by qRT-PCR, and the protein expression was tested by western blotting. At 24 h after transfection, cells were treated with TGF-β1 (PeproTech) at a concentration of 10 ng/ml for 48 h.

Adhesion assay

Wells of microwell plate were coated with matrix gel (BD Biosciences) at 37° C for 4 h, and were then blocked for 1 h with 1.2% BSA in PBS. Cells transfected with the *CCR2* 3′UTR or pSilencer 4.1 were suspended at concentration of 0.6×10^5 cells/well in serum-free medium. The colorimetric MTT-assay was used to determine the number of adherent cells after 1 h adhesion.

Wound healing assay

The wound healing assay was conducted as described previously (Chou et al., 2016). MCF-7 and MDA-MB-231 cells were seeded in six-well plates and transiently transfected with the *CCR2* 3′UTR or pSilencer 4.1. Cells were allowed to grow up to 90% confluency in complete medium. A vertical wound was made to cells with a sterile pipette tip, and the wounded monolayer was washed with PBS to remove cell debris, and serum-free medium was used to maintain cells. Phase-contrast images were taken of each sample at 0 h and 12 h (MDA-MB-231) or 24 h (MCF-7) at the same position with respect to the wound. The distances that cells migrated into wound surface were calculated for three different times. The migration rate was taken as $(D_0-D_t)/D_0$, where D_0 stands for the distance measured at 0 h and D_t refers to the distance measured at 12 h (MDA-MB-231) and 24 h (MCF-7).

Transwell migration and invasion assay

The migration assay was performed using a Transwell insert chamber (a pore size of 8 µm; Millipore) and the invasion assay was performed using BD Biosciences Matrigel invasion chambers (a pore size of 8 µm; BD Biosciences). After transfection, 10^5 cells in serum-free medium were placed into the upper chamber, and the lower chamber was filled with complete medium containing 20% FBS. For the migration assay, cells were allowed to migrate at 37°C for 24 h (MDA-MB-231) or 36 h (MCF-7). For the invasion assay, cells were allowed to invade at 37°C for 36 h (MDA-MB-231) or 48 h (MCF-7). The migrated or invaded cells were fixed in methanol for 30 min and stained with 0.1% Crystal Violet for 30 min. The stained cells were photographed, and the dye was eluted with glacial acetic acid and quantified by measuring with Microplate Reader [optical density (OD) at 570 nm].

Flow cytometric analysis of the cell cycle and apoptosis

Cells were harvested at 48 h after transfection. The cell cycle and apoptosis were analyzed by using a FACS caliber machine (Becton Dickinson) with a cell cycle assay kit (Vazyme) and apoptosis detection kit (Vazyme), respectively. The cell cycle distribution was determined via Propidium Iodide (PI) staining. A total of 20,000 gated events were acquired to assess the proportions of cells in different stages of the cell cycle and cell cycle profiles were calculated by using the ModFit LT 4.0 software. For the apoptosis assay, the cells were stained with Annexin V–FITC and PI. 10,000 cells were collected and FlowJo software was used to analyze the data, and the data were expressed as a percentage.

Luciferase reporter assay

To test whether miR-125b bound directly to the 3′UTR of *CCR2* mRNA, the pMIR-REPORT™ miRNA Expression Reporter Vector System (Applied Biosystems), consisting of an experimental firefly luciferase reporter vector and an associated β-gal reporter control plasmid were used. A portion of the 3′UTR of *CCR2* mRNA containing a wild-type (WT) or mutant (MUT) miR-125b-binding site was cloned respectively into the firefly luciferase reporter vector. For the luciferase assay, MCF-7 or MDA-MB-231 cells in 24-well plates were co-transfected with recombinant firefly luciferase reporter plasmids (CCR2-WT or CCR2-MUT), miR-125b mimics or

Journal of Cell Science (2017) 130, 3399-3413 doi:10.1242/jcs.202127

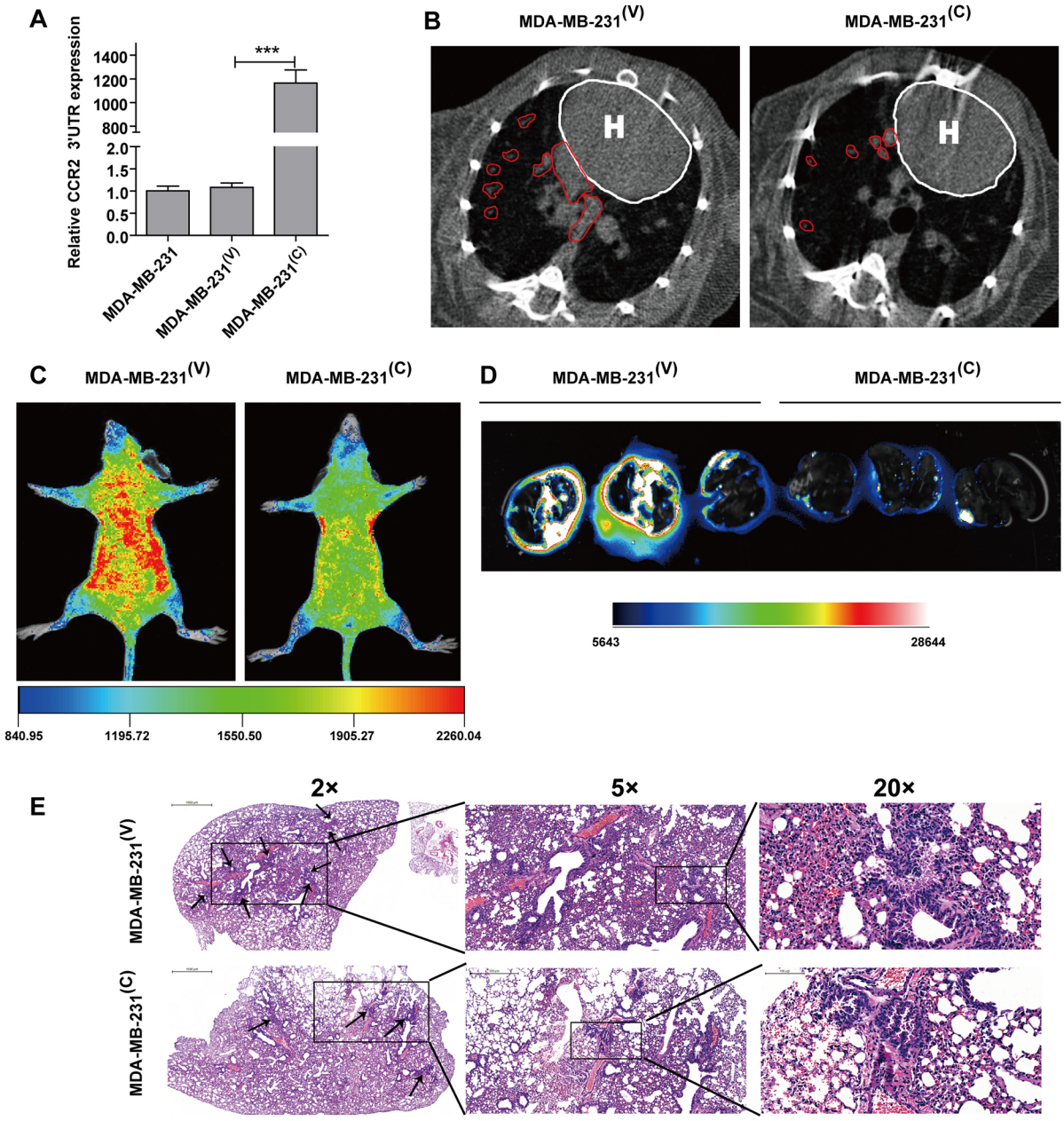

Fig. 8. The *CCR2* 3′UTR inhibits breast cancer metastasis in a xenograft model. (A) qRT-PCR analysis for expression of the *CCR2* 3′UTR in MDA-MB-231 cells stably transfected with an empty vector [MDA-MB-231$^{(V)}$] or the *CCR2* 3′UTR [MDA-MB-231$^{(C)}$]. Data are presented as mean±s.d., n=3. ***P<0.001 versus vector. (B) Six mice were intravenously injected with MDA-MB-231$^{(V)}$ or the MDA-MB-231$^{(C)}$ cells. After 8 weeks, animals were scanned by micro-CT and representative transverse images are shown. The heart is demarcated ('H') and the tumors are marked in red. (C) Representative bioluminescence images of mice injected with MDA-MB-231$^{(V)}$ cells or MDA-MB-231$^{(C)}$ cells. Ventral views are shown. (D) *Ex vivo* bioluminescent imaging showing the suppressive effect of the *CCR2* 3′UTR overexpression on pulmonary metastasis. The numbers on the color key in C and D indicate the bioluminescence signal (photons). (E) Representative histological images of lungs from the series described in C. Enlarged image of representative fields (magnifications, ×5 and ×20) are also shown.

mimics NC and β-gal reporter control plasmid using Lipofectamine 2000 reagent. Luciferase activity was measured according to the manufacturer's protocol and normalized to β-gal activity.

mRNA and miRNA quantification

Total RNA of cells after transfection was isolated by using TRIzol reagent (Invitrogen). cDNA was synthesized by using the M-MLV (Promega) following standard protocols. qRT-PCR was performed by using the Applied Biosystems StepOnePlus™ system. EzOmics SYBR qPCR mix and miRNA-125b qPCR kit were purchased from Biomics. MiR-125b levels were normalized to levels of U6 snRNA. The primers for various genes were designed and synthesized as follows:

GAPDH, 5′-AAGGTCGGAGTCAACGGATT-3′ and 5′-CTGGAA GATGGTGATGGGATT-3′; CCR2, 5′-CTGTCCACATCTCGTTCTCG GTTTA-3′ and 5′-CCCAAAGACCCACTCATTTGCAGC-3′; STARD13, 5′-AGCCCCTGCCTCAAAGTATT-3′ and 5′-ATGGGCGTCATCTGA TTCTC-3′; RhoA, 5′-GGACCCCAGAAGTCAAGCAT-3′ and 5′-GAGCAGCTCTCGTAGCCATT-3′; ROCK1, 5′-AACATGCTGCTGG ATAAATCTGG-3′, and 5′-TGTATCACATCGTACCATGCCT-3′; the *CCR2* 3′UTR: 5′-ATGCCTCATTACCTTGTG-3′ and 5′-CCATT CATCTGTGCCTGT-3′; the *STARD13* 3′UTR, 5′-TTAAAGCTAGATG AGGAGTTGCC -3′, and 5′-TTGACTTGGGGTCTGTAGTGATG-3′.

The relative gene expression level of each group was calculated by using the $2^{-\Delta\Delta ct}$ method.

Western blotting

Cells were harvested and lysed in buffer RIPA (Beyotime) on ice. Protein concentration was measured by using the BCA method. 30 µg protein of each sample was fractionated by 10% or 12% SDS-PAGE and transferred electrophoretically onto polyvinylidene difluoride membranes (Millipore). The membranes were blocked with 8% BSA in Tris-buffered saline with 0.1% Tween 20 at 37°C for 1 h and then blotted with primary antibodies overnight at 4°C. Antibodies against the following proteins were used: E-cadherin (ab40772), N-cadherin (ab76011) and vimentin (ab92547) (all 1:5000, Abcam); α-SMA (WL0002a; 1:1000, Wanleibio); CCR2 (12199), MLC (8505), pMLC^{S19} (3671) and RhoA (2117) (all 1:1000, Cell Signaling Technology); β-actin (TA-09 1:500, ZSGB-BIO); and STARD13 (AP19692c; 1:1000, ABGENT). After incubation with horseradish peroxidase (HRP)-conjugated secondary antibody (ZSGB-BIO), the protein bands were detected by using ECL chemiluminescence reagent (Tanon). Protein expression levels were quantified by density analysis using Quantity One Software and normalized to levels of β-actin.

RNA-binding protein immunoprecipitation assay

The RIP assay was performed using the Protein A/G Agarose Resin 4FF (YEASEN) following the manufacturer's protocol. Briefly, MDA-MB-231$^{(C)}$ cells (stably transfected with the *CCR2* 3′UTR), MDA-MB-231$^{(V)}$ cells (stably transfected with an empty vector) and MDA-MB-231$^{(S)}$ (stably transfected with STARD13 3′UTR) cells were lysed with NP-40 lysis buffer (Beyotime). Then, 100 µl cells extract was incubated with NP-40 buffer containing Protein A/G Agarose Resin 4FF conjugated to human anti-Ago antibody (Cell Signaling Technology) at 4°C overnight. Agarose resin was isolated by centrifugation and incubated with proteinase K (Beyotime) to dissociate the Ago2–RNA complex from the agarose resin. qRT-PCR was performed to detect *CCR2*, *STARD13* and miR-125b levels.

RhoA GTPase assay

Cells were assayed for RhoA GTPase activity by performing a RhoA G-LISA (Cytoskeleton) according to the commercial protocol. Briefly, lysates were prepared and lysate protein concentration was measured. Lysis buffer was then added to equalize the cell extracts to give identical protein concentrations in each sample. Samples were incubated in the wells provided and then managed following the technical guide. Absorbance at 490 nm was measured using a microplate spectrophotometer.

Immunofluorescence and F-actin visualization

Cells were fixed in 4% paraformaldehyde for 20 min, permeabilized with 0.2% Triton X-100 for 20 min at 4°C, and blocked with 3% BSA in PBS for 1 h at room temperature. For immunofluorescence, appropriate primary antibodies [E-cadherin (ab40772), N-cadherin (ab76011) (both 1:100, Abcam) and vimentin (ab92547, 1:200, Abcam)] were used to blot overnight at 4°C and FITC-conjugated secondary antibody was used. For F-actin visualization, F-actin was stained with Rhodamine–phalloidin (Cytoskeleton) for 30 min at room temperature. The nuclei were stained with DAPI for 30 min and observed through confocal microscopy. Cells were captured by adopting confocal laser scanning. Images were analyzed using OLYMPUS FLUOVIEW ver.3.0 Viewer software and the fluorescence intensity was quantified by using Image J software.

In vivo metastasis study

All experiments were carried out under the ethical approval of Ethics Committee for Animal Experimentation of China Pharmaceutical University. Six-week-old female nude mice were purchased from the Model Animal Research Center of Nanjing University. Intravenous injection with MDA-MB-231 cells that were stably overexpressed the *CCR2* 3′UTR or empty vector was performed, and 5×10^6 cells in 150 µl PBS were injected into six animals per group. At 8 weeks after injection, animals were scanned using the SkyScan 1176 micro-CT scanner. For bioluminescent analysis, Nano-Glo^{TM} substrate containing furimazine (20 µg in 100 µl PBS, Promega) was injected intraperitoneally into mice before imaging. Images of *in vivo* tumor growth and *ex vivo* lung metastasis were taken using the Carestream noninvasive optical imaging system. Mice were killed, and then lungs were sectioned and stained with H&E.

Statistical analysis

The data are presented as the mean±s.d. and statistical evaluation for data analysis was determined by using an unpaired Student's test. $P<0.05$ was considered to indicate a statistically significant result. *$P<0.05$, **$P<0.01$, ***$P<0.001$; ns indicates no significant differences from control. Survival analysis was performed using the Kaplan–Meier plotter tool (http://kmplot.com/analysis/).

Competing interests

The authors declare no competing or financial interests.

Author contributions

Conceptualization: L.Z., T.X.; Methodology: J.H., X.L., X.G., Q.G., Y.X., L.Z.; Software: J.H., X.G., Q.G., C.X., Z.Z., L.Z.; Validation: J.H., Y.X., T.X.; Formal analysis: J.H., Q.G., C.X.; Investigation: J.H., X.L.; Resources: L.Z., T.X.; Data curation: X.L., X.G.; Writing - original draft: J.H.; Writing - review & editing: X.L., Z.Z.; Supervision: Y.X.; Project administration: L.Z., T.X.; Funding acquisition: T.X.

Funding

This work was supported by the National Major Special Program of New Drug Research and Development (no. 2013ZX09301303-005), the Priority Academic Program Development (PAPD) of Jiangsu Higher Education Institutions and Qing Lan Project, National Natural Science Foundation of China (no. 81372331), and the Fundamental Research Funds for the Central Universities (no. 2015ZD004).

Supplementary information

Supplementary information available online at
http://jcs.biologists.org/lookup/doi/10.1242/jcs.202127.supplemental

References

Biddle, A. and Mackenzie, I. C. (2012). Cancer stem cells and EMT in carcinoma. *Cancer Metastasis Rev.* **31**, 285-293.

Bosson, A. D., Zamudio, J. R. and Sharp, P. A. (2014). Endogenous miRNA and target concentrations determine susceptibility to potential ceRNA competition. *Mol. Cell* **56**, 347-359.

Cesana, M., Cacchiarelli, D., Legnini, I., Santini, T., Sthandier, O., Chinappi, M., Tramontano, A. and Bozzoni, I. (2011). A long noncoding RNA controls muscle differentiation by functioning as a competing endogenous RNA. *Cell* **147**, 358-369.

Ching, Y.-P., Wong, C.-M., Chan, S.-F., Leung, T. H.-Y., Ng, D. C.-H., Jin, D.-Y. and Ng, I. O. (2003). Deleted in liver cancer (DLC) 2 encodes a RhoGAP protein with growth suppressor function and is underexpressed in hepatocellular carcinoma. *J. Biol. Chem.* **278**, 10824-10830.

Chou, J., Wang, B., Zheng, T., Li, X., Zheng, L., Hu, J., Zhang, Y., Xing, Y. and Xi, T. (2016). MALAT1 induced migration and invasion of human breast cancer cells by competitively binding miR-1 with cdc42. *Biochem. Biophys. Res. Commun.* **472**, 262-269.

de Sousa Abreu, R., Penalva, L. O., Marcotte, E. M. and Vogel, C. (2009). Global signatures of protein and mRNA expression levels. *Mol. Biosyst.* **5**, 1512-1526.

Denzler, R., Agarwal, V., Stefano, J., Bartel, D. P. and Stoffel, M. (2014). Assessing the ceRNA hypothesis with quantitative measurements of miRNA and target abundance. *Mol. Cell* **54**, 766-776.

Denzler, R., McGeary, S. E., Title, A. C., Agarwal, V., Bartel, D. P. and Stoffel, M. (2016). Impact of microRNA levels, target-site complementarity, and cooperativity on competing endogenous RNA-regulated gene expression. *Mol. Cell* **64**, 565-579.

Fang, W. B., Jokar, I., Zou, A., Lambert, D., Dendukuri, P. and Cheng, N. (2012). CCL2/CCR2 chemokine signaling coordinates survival and motility of breast cancer cells through Smad3 protein- and p42/44 Mitogen-activated Protein Kinase (MAPK)-dependent mechanisms. *J. Biol. Chem.* **287**, 36593-36608.

Fang, L., Du, W. W., Yang, X., Chen, K., Ghanekar, A., Levy, G., Yang, W., Yee, A. J., Lu, W.-Y., Xuan, J. W. et al. (2013). Versican 3′-untranslated region (3′-UTR) functions as a ceRNA in inducing the development of hepatocellular carcinoma by regulating miRNA activity. *FASEB J.* **27**, 907-919.

Gilkes, D. M., Xiang, L., Lee, S. J., Chaturvedi, P., Hubbi, M. E., Wirtz, D. and Semenza, G. L. (2014). Hypoxia-inducible factors mediate coordinated RhoA-ROCK1 expression and signaling in breast cancer cells. *Proc. Natl. Acad. Sci. USA* **111**, E384-E393.

Győrffy, B., Lanczky, A., Eklund, A. C., Denkert, C., Budczies, J., Li, Q. and Szallasi, Z. (2010). An online survival analysis tool to rapidly assess the effect of 22,277 genes on breast cancer prognosis using microarray data of 1,809 patients. *Breast Cancer Res. Treat.* **123**, 725-731.

Izumi, K., Fang, L.-Y., Mizokami, A., Namiki, M., Li, L., Lin, W.-J. and Chang, C. (2013). Targeting the androgen receptor with siRNA promotes prostate cancer metastasis through enhanced macrophage recruitment via CCL2/CCR2-induced STAT3 activation. *EMBO Mol. Med.* **5**, 1383-1401.

Jiao, A., Sui, M., Zhang, L., Sun, P., Geng, D., Zhang, W., Wang, X. and Li, J. (2016). MicroRNA-200c inhibits the metastasis of non-small cell lung cancer cells by targeting ZEB2, an epithelial-mesenchymal transition regulator. *Mol. Med. Rep.* **13**, 3349-3355.

Karreth, F. A., Tay, Y., Perna, D., Ala, U., Tan, S. M., Rust, A. G., DeNicola, G., Webster, K. A., Weiss, D., Perez-Mancera, P. A. et al. (2011). In vivo identification of tumor- suppressive PTEN ceRNAs in an oncogenic BRAF-induced mouse model of melanoma. *Cell* **147**, 382-395.

Kong, W., Yang, H., He, L., Zhao, J.-J., Coppola, D., Dalton, W. S. and Cheng, J. Q. (2008). MicroRNA-155 is regulated by the transforming growth factor beta/Smad pathway and contributes to epithelial cell plasticity by targeting RhoA. *Mol. Cell. Biol.* **28**, 6773-6784.

Kumar, M. S., Armenteros-Monterroso, E., East, P., Chakravorty, P., Matthews, N., Winslow, M. M. and Downward, J. (2014). HMGA2 functions as a competing endogenous RNA to promote lung cancer progression. *Nature* **505**, 212-217.

Lee, E. Y., Chung, C. H., Khoury, C. C., Yeo, T. K., Pyagay, P. E., Wang, A. and Chen, S. (2009). The monocyte chemoattractant protein-1/CCR2 loop, inducible by TGF-beta, increases podocyte motility and albumin permeability. *Am. J. Physiol. Renal Physiol.* **297**, F85-F94.

Leung, T. H.-Y., Ching, Y.-P., Yam, J. W. P., Wong, C.-M., Yau, T.-O., Jin, D.-Y. and Ng, I. O.-L. (2005). Deleted in liver cancer 2 (DLC2) suppresses cell transformation by means of inhibition of RhoA activity. *Proc. Natl. Acad. Sci. USA* **102**, 15207-15212.

Li, J., Yuan, J., Yuan, X., Zhao, J., Zhang, Z., Weng, L. and Liu, J. (2016a). MicroRNA-200b inhibits the growth and metastasis of glioma cells via targeting ZEB2. *Int. J. Oncol.* **48**, 541-550.

Li, X., Zheng, L., Zhang, F., Hu, J., Chou, J., Liu, Y., Xing, Y. and Xi, T. (2016b). STARD13-correlated ceRNA network inhibits EMT and metastasis of breast cancer. *Oncotarget* **7**, 23197-23211.

Lim, S. Y., Yuzhalin, A. E., Gordon-Weeks, A. N. and Muschel, R. J. (2016). Targeting the CCL2-CCR2 signaling axis in cancer metastasis. *Oncotarget* **7**, 28697-28710.

Lin, Y., Chen, N.-T., Shih, Y.-P., Liao, Y.-C., Xue, L. and Lo, S. H. (2010). DLC2 modulates angiogenic responses in vascular endothelial cells by regulating cell attachment and migration. *Oncogene* **29**, 3010-3016.

Liu, K., Yan, Z., Li, Y. and Sun, Z. (2013). Linc2GO: a human LincRNA function annotation resource based on ceRNA hypothesis. *Bioinformatics* **29**, 2221-2222.

Nitzan, M., Steiman-Shimony, A., Altuvia, Y., Biham, O. and Margalit, H. (2014). Interactions between distant ceRNAs in regulatory networks. *Biophys. J.* **106**, 2254-2266.

Papageorgis, P., Ozturk, S., Lambert, A. W., Neophytou, C. M., Tzatsos, A., Wong, C. K., Thiagalingam, S. and Constantinou, A. I. (2015). Targeting IL13Ralpha2 activates STAT6-TP63 pathway to suppress breast cancer lung metastasis. *Breast Cancer Res.* **17**, 98.

Qian, B.-Z., Li, J., Zhang, H., Kitamura, T., Zhang, J., Campion, L. R., Kaiser, E. A., Snyder, L. A. and Pollard, J. W. (2011). CCL2 recruits inflammatory monocytes to facilitate breast-tumour metastasis. *Nature* **475**, 222-225.

Salmena, L., Poliseno, L., Tay, Y., Kats, L. and Pandolfi, P. P. (2011). A ceRNA hypothesis: the rosetta stone of a hidden RNA language? *Cell* **146**, 353-358.

Stricker, J., Falzone, T. and Gardel, M. L. (2010). Mechanics of the F-actin cytoskeleton. *J. Biomech.* **43**, 9-14.

Sui, X., Wang, X., Han, W., Li, D., Xu, Y., Lou, F., Zhou, J., Gu, X., Zhu, J., Zhang, C. et al. (2015). MicroRNAs-mediated cell fate in triple negative breast cancers. *Cancer Lett.* **361**, 8-12.

Sumazin, P., Yang, X., Chiu, H.-S., Chung, W.-J., Iyer, A., Llobet-Navas, D., Rajbhandari, P., Bansal, M., Guarnieri, P., Silva, J. et al. (2011). An extensive microRNA-mediated network of RNA-RNA interactions regulates established oncogenic pathways in glioblastoma. *Cell* **147**, 370-381.

Tang, F., Zhang, R., He, Y., Zou, M., Guo, L. and Xi, T. (2012). MicroRNA-125b induces metastasis by targeting STARD13 in MCF-7 and MDA-MB-231 breast cancer cells. *PLoS ONE* **7**, e35435.

Tay, Y., Kats, L., Salmena, L., Weiss, D., Tan, S. M., Ala, U., Karreth, F., Poliseno, L., Provero, P., Di Cunto, F. et al. (2011). Coding-independent regulation of the tumor suppressor PTEN by competing endogenous mRNAs. *Cell* **147**, 344-357.

Tay, Y., Rinn, J. and Pandolfi, P. P. (2014). The multilayered complexity of ceRNA crosstalk and competition. *Nature* **505**, 344-352.

Yang, J., Lv, X., Chen, J., Xie, C., Xia, W., Jiang, C., Zeng, T., Ye, Y., Ke, L., Yu, Y. et al. (2016). CCL2-CCR2 axis promotes metastasis of nasopharyngeal carcinoma by activating ERK1/2-MMP2/9 pathway. *Oncotarget* **7**, 15632-15647.

Zheng, L., Li, X., Gu, Y., Lv, X. and Xi, T. (2015). The 3′UTR of the pseudogene CYP4Z2P promotes tumor angiogenesis in breast cancer by acting as a ceRNA for CYP4Z1. *Breast Cancer Res. Treat.* **150**, 105-118.